The QME AERI LBLRTM: A Closure Experiment for Downwelling High Spectral Resolution Infrared Radiance

D. D. TURNER,* D. C. TOBIN,+ S. A. CLOUGH,# P. D. BROWN,# R. G. ELLINGSON,@ E. J. MLAWER,# R. O. KNUTESON,+ H. E. REVERCOMB,+ T. R. SHIPPERT,* W. L. SMITH,& AND M. W. SHEPHARD#

*Pacific Northwest National Laboratory, Richland, Washington
+Cooperative Institute for Meteorological Satellite Studies, University of Wisconsin—Madison, Madison, Wisconsin
#Atmospheric and Environmental Research, Inc., Lexington, Massachusetts
@Florida State University, Tallahassee, Florida
&NASA Langley Research Center, Hampton, Virginia

(Manuscript received 13 June 2003, in final form 22 April 2004)

ABSTRACT

Research funded by the U.S. Department of Energy's Atmospheric Radiation Measurement (ARM) program has led to significant improvements in longwave radiative transfer modeling over the last decade. These improvements, which have generally come in small incremental changes, were made primarily in the water vapor self- and foreign-broadened continuum and the water vapor absorption line parameters. These changes, when taken as a whole, result in up to a 6 W m^{-2} improvement in the modeled clear-sky downwelling longwave radiative flux at the surface and significantly better agreement with spectral observations. This paper provides an overview of the history of ARM with regard to clear-sky longwave radiative transfer, and analyzes remaining related uncertainties in the ARM state-of-the-art Line-by-Line Radiative Transfer Model (LBLRTM).

A quality measurement experiment (QME) for the downwelling infrared radiance at the ARM Southern Great Plains site has been ongoing since 1994. This experiment has three objectives: 1) to validate and improve the absorption models and spectral line parameters used in line-by-line radiative transfer models, 2) to assess the ability to define the atmospheric state, and 3) to assess the quality of the radiance observations that serve as ground truth for the model. Analysis of data from 1994 to 1997 made significant contributions to optimizing the QME, but is limited by small but significant uncertainties and deficiencies in the atmospheric state and radiance observations. This paper concentrates on the analysis of QME data from 1998 to 2001, wherein the data have been carefully selected to address the uncertainties in the 1994–97 dataset. Analysis of this newer dataset suggests that the representation of self-broadened water vapor continuum absorption is 3%–8% too strong in the 750–1000 cm^{-1} region. The dataset also provides information on the accuracy of the self- and foreign-broadened continuum absorption in the 1100–1300 cm^{-1} region. After accounting for these changes, remaining differences in modeled and observed downwelling clear-sky fluxes are less than 1.5 W m^{-2} over a wide range of atmospheric states.

1. Introduction

Longwave and solar radiative transfer are the prime physical mechanisms that drive the circulation and temperature structure of the atmosphere, and radiative processes play a central role in most climate change mechanisms (Luther 1984). Full treatment of the radiative transfer in a global climate model (GCM[1]) is prohibitively expensive, and thus parameterization is required to account for the radiant energy transport in GCMs. Detailed radiative transfer models that incorporate all of the known physics, such as line-by-line models, are typically used to construct significantly faster radiation models to calculate radiative fluxes in GCMs. The line-by-line model used to build these faster models must be accurate, as even 1% changes in radiation are significant for climate (Ellingson and Wiscombe 1996).

Recognizing the importance of radiative transfer in climate modeling, the World Climate Research Program, the International Radiation Commission, and the U.S. Department of Energy (DOE) initiated an international radiative transfer model study. The initial focus of the Intercomparison of Radiation Codes in Climate Models (ICRCCM) was on clear-sky scenes, which are inherently easier to model than cloudy scenes. The differences in computed longwave radiative fluxes for the clear-sky atmospheres approached 70 W m^{-2} (Ellingson et al. 1991; Ellingson and Wiscombe 1996). Even the line-by-line models differed by tens of watts per square

[1] A list of acronyms is given in the appendix.

Corresponding author address: David D. Turner, Climate Physics Group, Pacific Northwest National Laboratory, MS K9-24, P.O. Box 999, Richland, WA 99352.
E-mail: dave.turner@pnl.gov

meter, due largely to different formulations of the water vapor continuum absorption. If the different line-by-line models used the same cutoff point for line absorption and the same continua model, the differences were less than 1% in the downwelling flux. However, due to remaining uncertainties in the *absolute* accuracy of line absorption parameters, line shape, and continua used in these models (Luther et al. 1988), ICRCCM recommended that a dedicated field program be organized to simultaneously measure radiance at high spectral resolution along with the atmospheric state data (profiles of temperature, water vapor, etc.) needed for validation of the radiance calculations (Ellingson and Fouquart 1991). The DOE Atmospheric Radiation Measurement (ARM) program (Stokes and Schwartz 1994) was designed, in part, to address this recommendation.

This paper discusses the quality measurement experiment (QME) that compares observations and calculations of downwelling longwave high spectral resolution radiance at the ARM Southern Great Plains (SGP) Cloud and Radiation Testbed (CART) site over a long-term dataset. S.A. Clough proposed the concept and implementation plan for this QME (Clough et al. 1994). The QME has been used to: 1) validate and improve absorption models and spectral line parameters used in a line-by-line model, 2) assess the ability to define the atmospheric state used in the model calculation, and 3) assess the quality of the radiance observations themselves. The design of the QME allows all three of these aspects to be addressed simultaneously. This QME has been ongoing since 1994, when the full suite of required instruments (with the exception of the Raman lidar) were first made operational. While the QME can be used to investigate the absorption due to a variety of trace gases, the focus of this paper is on the accuracy of the water vapor observations and the representation of water vapor continuum absorption because of the large impact this absorption has on the radiative flux calculations.

The paper begins by introducing the line-by-line radiative transfer model and the instruments that are used in this QME in section 2. Section 3 discusses the QME results from 1994–97, highlighting some of the uncertainties in both the radiance and atmospheric state observations. Analysis of the early QME results led to a series of focused intensive observation periods (IOPs) that have reduced the uncertainties in these observations. A new QME dataset, compiled using data from 1998 to 2001 to address the uncertainties highlighted in the early QME dataset, is discussed in section 4. Section 5 analyzes the new QME dataset in detail, looking at the impact on the radiance residuals (observed − calculated) to errors in total column water vapor, as well as the effect of aerosols. The paper concludes by summarizing the large improvement in longwave radiative transfer modeling that the ARM program has made over the last decade.

2. Model and instrumentation

The ARM SGP CART site near Lamont, Oklahoma, has a wide variety of instrumentation designed to meet ARM's goal of collecting a long term (>10 yr) dataset that can be used to improve GCMs. Of particular importance to the QME are the Atmospheric Emitted Radiance Interferometer (AERI), radiosondes, microwave radiometer (MWR), Raman lidar, and micropulse lidar (MPL). This section describes these sensors, and the radiative transfer model used in the QME comparisons.

a. Line-by-Line Radiative Transfer Model

The Line-By-Line Radiative Transfer Model (LBLRTM; Clough et al. 1992; Clough and Iacono 1995) used in this QME is based upon the Fast Atmospheric Signature Code (FASCODE) model (Clough et al. 1985), and achieves high accuracy with computational efficiency. All of the parameters of the High-Resolution Transmission (HITRAN) molecular absorption database (Rothman et al. 1998, 2003) are used, including the coefficient for the self-broadening of water vapor, half-width dependence on temperature, and the pressure shift coefficient. A Voigt line shape is used for all pressures, with a line cutoff at 25 cm^{-1} from line center. A consistently defined water vapor continuum model (CKD; Clough et al. 1989) incorporates both the self-broadened and foreign-broadened components. In the longwave, the LBLRTM also includes continua representation of absorption by carbon dioxide, oxygen, and nitrogen. The LBLRTM has been used to generate the rapid radiative transfer model (RRTM; Mlawer et al. 1997) that is used in various other models (Morcrette et al. 1998; Iacono et al. 2000; Warner and Ellingson 2000). Therefore, it is important to validate the LBLRTM with direct observations.

This paper discusses output from several versions of the LBLRTM. The different models, including the details of the differences between them, and the line parameter databases are available from Atmospheric and Environmental Research Incorporated's (AER) Radiative Transfer Working Group's Web site (http://rtweb.aer.com).

b. Atmospheric Emitted Radiance Interferometer

The AERI is a fully automated, ground-based, passive interferometer that measures high spectral resolution downwelling infrared radiance from 500 to 3000 cm^{-1} (19 to 3.3 μm). It was developed for the ARM program by the University of Wisconsin—Madison as a ground-based version of the High-Spectral-Resolution Infrared Sounder (HIS; Smith et al. 1993; Revercomb et al. 1993), and was used during the Spectral Radiance Experiment (SPECTRE; Ellingson and Wiscombe 1996) and many other field programs. The instrument is based around a commercially available interferometer (Mi-

chelson series MB100[2] from Bomem, Inc. of Quebec City, Quebec, Canada). The maximum optical path delay is approximately ±1 cm, resulting in a maximum unapodized spectral resolution of ~0.5 cm^{-1}.

The calibration goal for the AERI is to observe downwelling atmospheric radiance with an accuracy of better than 1% of the ambient (near surface) radiance (Revercomb et al. 1993). Two well-characterized blackbody targets are used to achieve this accuracy, and a rotating gold-plated scene mirror is used to direct radiation from the target (either the sky or one of the blackbodies) into the interferometer. A typical measurement cycle consists of a 3-min sky view period, followed by a 2-min view period for each of the blackbody targets. The blackbodies are high-emissivity (greater than 0.995) targets that contain accurate National Institute of Standards and Technology (NIST) traceable temperature sensors (Minnett et al. 2001). The temperature of one of the blackbodies is fixed at 60°C, while the other is allowed to float at the ambient temperature. One of the advantages to using an ambient calibration target is that much of the emission measured by the AERI is from the atmosphere very close to the instrument. Therefore, the calibration error is very small for temperatures very near the surface temperature.

The instrument measures interferograms, from which complex radiance spectra are computed using Fourier transforms. Spectra observed from the blackbodies at known temperatures are used to calibrate the atmospheric spectrum following Revercomb et al. (1988). The calibration procedure also accounts for detector nonlinearity, spectral calibration, including the removal of interferometer self-apodization effects, and spectral scale normalization to standardize spectra from different instruments. A typical example of a side-by-side comparison of two AERI instruments is shown in Fig. 1. The radiance differences are smaller than 0.5 mW m^{-2} sr^{-1} cm^{-1} [hereafter referred to as a radiance unit (RU)]. More details on the AERI instrument, how it is calibrated, and the uncertainties in its observations are provided by Knuteson et al. (2004a,b).

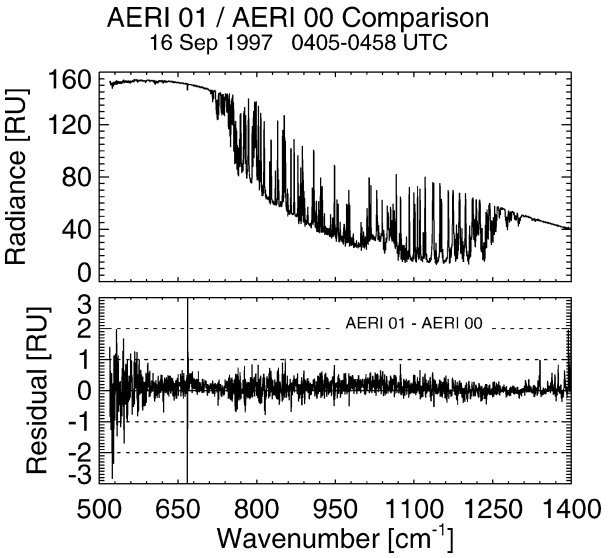

FIG. 1. An intercomparison of spectra collected by the operational ARM AERI (01) and the original prototype (AERI 00) on 16 Sep 1997. The radiance difference between the two observations is less than 0.5 mW m^{-2} sr^{-1} cm^{-1} (called an RU) across the spectrum.

c. Microwave radiometer

The MWRs used by the ARM program are Radiometrics WVR-1100 radiometers. They are two-channel units that measure downwelling radiation at 23.8 and 31.4 GHz. Water vapor emission dominates the 23.8-GHz signal. This channel is chosen to be near the hinge point (i.e., the spectral frequency where the emission is insensitive to changes in pressure and knowledge of the spectral line width) of the 22.2-GHz water vapor line. Cloud liquid water, which emits in a broad continuum that increases with frequency, dominates the 31.4-GHz signal. Physical or statistical retrievals can be performed on the two observed sky brightness temperatures to retrieve precipitable water vapor (PWV) and cloud liquid water in the atmospheric column. Laboratory measurements of the Stark effect have enabled the strength of the 22.2-GHz water vapor absorption line to be measured with great accuracy (Clough et al. 1973). Therefore, as suggested by Clough et al. (1996), the PWV retrieved from accurate observations on this line have been used as a constraint on the total amount of water vapor in the column. This has been shown to greatly reduce the uncertainty in the calibration of the moisture sensor of the radiosonde, as evidenced by significantly less variance in the downwelling longwave observed minus calculated residuals (Clough et al. 1996; Turner et al. 1998; Clough et al. 1999; Turner et al. 2003).

Operationally, the ARM program uses the ''Liebe87'' microwave absorption model (Liebe and Layton 1987) in a quasi-statistical retrieval to retrieve PWV and cloud liquid water for each 20-s observation. The retrieval method, which is summarized here, is provided in Liljegren and Lesht (1996). A historical database of radiosondes from the SGP region is used to drive the Liebe87 model to compute opacity and mean radiating temperatures in each of the two channels. Averages of the mean radiating temperature have been created for each month of the year, and these average values are used to derive linear relationships between the opacity in each channel with the PWV and cloud liquid water. These linear relationships are then used to retrieve PWV and cloud liquid water from the observed sky brightness temperatures, which are converted to opacity with the use of the appropriate monthly averaged mean radiating temperature.

Accurate radiometric calibration of the MWR is cru-

[2] Mention of commercial products does not indicate endorsement by the Department of Energy or its contractors.

cial to the accurate retrieval of PWV and cloud liquid water. The ARM MWRs have a single ambient blackbody target, which is viewed as part of every sky view sequence. The blackbody is viewed both normally and when a noise diode, which inserts a fixed amount of additional energy into the system, is turned on. These two values allow the gain of the instrument to be determined, provided that the ''temperature'' of the noise diode is known. To determine this temperature, the ARM radiometers use the tip-curve method (Han et al. 1994), whereby the instrument takes observations at a series of angles on either side of zenith in a vertical plane. If the sky is horizontally homogeneous, then the opacity, which varies linearly with airmass (secant of the zenith angle), can be used to determine the gain of the system. This process allows the temperature of the noise diode to be determined from the raw voltage measurements made by the system. An automated routine was developed which collects tip-curve data whenever the sky is deemed to be clear and homogeneous (otherwise the system is placed in a zenith-only mode). This routine processes these tip curves, allowing the calibration of the instrument to be maintained continuously (Liljegren 2000). This automated routine is able to maintain the calibration to 0.2–0.3-K rms, which corresponds to an uncertainty in PWV of less than 0.3 mm. This autocalibration software was installed on the SGP MWRs in October 1998.

d. Radiosondes

The ARM program uses the Vaisala RS80-H radiosonde for all of its soundings.[3] These radiosondes incorporate the H-humicap capacitive moisture sensor that is more sensitive and stable than the more commonly used A-humicap (Antikainen and Paukkunen 1994). These radiosondes measure temperature, relative humidity, pressure, and wind speed and direction, which is processed with the standard quality control software provided by the manufacturer that filters, edits, and interpolates the data and output it at 2-s resolution. ARM typically launches three to five radiosondes per day from its central facility at the SGP CART site at various times of the day, and up to eight radiosondes per day are launched during IOPs.

Recent work by several groups has shown that a dry bias exists in Vaisala humidity measurements (Guichard et al. 2000; Wang et al. 2002; Turner et al. 2003). Laboratory analyses have established that this dry bias is due to chemical contamination of the capacitive moisture sensor, and a correction has been developed to account for this bias (Wang et al. 2002). The correction also accounts for small errors in the temperature dependence of the sensor and in the basic humidity calibration model, but these components are much smaller than the chemical contamination component for the RS80-H (Lesht 1999). However, analysis of over 2000 radiosondes launched from the ARM SGP site have demonstrated that there is a large sonde-to-sonde variation in the calibration of the water vapor observations (peak-to-peak differences greater than 25%) that is not accounted for by this correction (Revercomb et al. 1998; Turner et al. 2003; Revercomb et al. 2003). Turner et al. (2003) also demonstrate that Vaisala radiosondes exhibit a significant (~4% in PWV) diurnal bias that is not accounted for by the correction. Additionally, this correction introduces a small, height-dependent bias in the lower troposphere in the corrected radiosondes (Turner et al. 2003). For these reasons, ARM does not apply this correction to its radiosonde data operationally.

The dry bias and the sonde-to-sonde variability make these data problematic for use in the QME. Clough et al. (1996) showed that the differences in the PWV measured by the sonde and MWR were well correlated with the radiance residuals between the AERI and the LBLRTM. Launching two radiosonde sensor packages on the same balloon during special water vapor IOPs at the SGP CART site demonstrated that the differences are, to first order, due to a height-independent calibration factor error in the radiosonde moisture profiles (Revercomb et al. 2003). Therefore, a height-independent scale factor, which is the ratio of the PWV observed by the MWR and radiosonde, is computed and the radiosonde's mixing ratio profile is multiplied by this scale factor. This has been shown to significantly reduce the sonde-to-sonde variability in the moisture observations, remove the diurnal bias, and account for the dry bias in the lower troposphere (Turner et al. 2003). The RS80 radiosondes also exhibit a significant time-lag error in humidity at cold temperatures, which is significant in the upper troposphere (Miloshevich et al. 2003), but downwelling infrared radiance at the surface is not very sensitive to these errors.

e. Raman lidar

The Raman lidar at the SGP site was designed to meet the ARM program's goals of being able to profile water vapor in the boundary layer throughout the diurnal cycle (Goldsmith et al. 1998). It is the first fully automated atmospheric Raman lidar system, initially deployed in 1996 and becoming truly operational in April 1998. It operates by transmitting nominally 350-mJ pulses of 355-nm light into the atmosphere at 30 Hz. The backscattered light is collected with a 61-cm telescope, and the time of the flight of the backscatter is recorded at three wavelengths with 39-m vertical resolution. The inelastic backscatter at 408 and 387 nm due to the Raman shifts of water vapor and nitrogen, respectively, is measured, as well as the elastic backscatter at 355 nm. The backscatter at 355 nm is split into the co- and cross-

[3] After April 2001, the ARM program began using the newer Vaisala RS90 radiosonde package. However, all radiosondes used in this analysis are RS80-H radiosondes.

polarized components (with respect to the outgoing laser beam) providing sensitivity to aspherical particles such as ice crystals. A dual field of view, narrow bandpass approach permits daytime profiling in the boundary layer without compromising the ability of the Raman lidar to profile throughout the troposphere (in cloud-free cases) at night.

Profiles of water vapor mixing ratio, aerosol scattering ratio, and linear depolarization ratio can be derived from these raw signals. Additionally, profiles of relative humidity, aerosol backscatter coefficient, and aerosol extinction coefficient can also be derived if a temperature profile is available. Automated algorithms have been developed to retrieve all of these products routinely (Turner et al. 2002). Uncertainties in the Raman cross section of water vapor preclude the radiometric calibration of the Raman lidar at this time, and thus the calibration factor is determined such that the PWV derived from the water vapor mixing ratio agrees with the MWR (Turner and Goldsmith 1999; Turner et al. 2002). The sensitivity of the Raman lidar depolarization ratio allows all clouds that are radiatively significant in the infrared to be detected, including subvisual cirrus.

f. Micropulse lidar

The MPL is a relatively simple (compared to the ARM Raman lidar) cloud and aerosol lidar. It was developed in the early 1990s at the NASA Goddard Space Flight Center (Spinhirne 1993), and the first MPL was deployed at the SGP site in 1993. It uses a solid-state laser to transmit light at 523 nm with low pulse energies (20 μJ) at a high repetition rate (2.5 kHz). The outgoing beam is expanded by a shared transmit/receive telescope to achieve eye safety. Only the elastic backscatter at the laser wavelength is detected, and the instrument is not polarization sensitive. Like the Raman lidar, a narrow field of view and a narrow bandpass interference filter are used to limit the solar noise, allowing the instrument to profile aerosols and clouds throughout the troposphere for the entire diurnal cycle. Instrument details and basic data processing are described in Campbell et al. (2002).

3. QME dataset: 1994–97

To evaluate the performance of any model, the uncertainties in the atmospheric state data that are input into the model, as well as in the observed radiance data, must be well understood. A set of simultaneous AERI observations and radiosonde profiles were compiled between April 1994 and December 1997. The LBLRTM computes absorption due to gases; clouds and aerosols are not treated in a typical LBLRTM run. Therefore, the MPL was used to identify cloudy scenes in the QME dataset, which were subsequently removed. A large number of analyses using this dataset have been performed (Clough et al. 1994, 1996, 1999; Brown et al. 1997; Ellingson and Shen 1997; Shen and Ellingson 1996; Revercomb et al. 1994, 1996; Turner et al. 1998). However, we suspect that several cases remain in the dataset that are not clear sky. These cases were contaminated by very thin cirrus, as the low pulse energies of the MPL could make detection of tenuous cirrus difficult, especially in the daytime when the solar background is large.

This dataset also highlighted the large uncertainty in the water vapor observations made by the radiosondes. Analysis of the observed minus calculated radiance residuals demonstrated a good correlation with the difference in the PWV observed by the MWR and the radiosonde, when the unscaled radiosonde profiles were used as input into the LBLRTM (Clough et al. 1996). However, there was significant scatter in the residuals, and it was determined that the uncertainty in the accuracy of the water vapor profiles was the limiting factor in improving the radiative transfer model (Ellingson and Shen 1997; Revercomb et al. 2003). This led to a series of IOPs at the ARM SGP site to characterize ARM's water vapor observations and improve them (Revercomb et al. 2003). These water vapor IOPs occurred in September 1996, September–October 1997, and September–October 2000. Data collected during these IOPs demonstrated that the sonde-to-sonde variability is due primarily to calibration errors that are height independent in the lower troposphere, and that MWR PWV observations could be used to scale the radiosonde's moisture profile to decrease the variability (Clough et al. 1999; Turner et al. 2003). This resulted in a significant decrease (factor of approximately 2 in rms) in the AERI − LBLRTM radiance residuals.

Analysis of the 1996 and 1997 water vapor IOP datasets also highlighted the importance of frequent tip-curve data in the MWR calibration, and identified some phenomenon that can affect these scanning data (Han and Westwater 2000). Corrections for these phenomena, such as accounting for the antenna beamwidth, were implemented as part of a routine to automatically calibrate the ARM MWRs (Liljegren 2000). This software was installed on the MWRs in October 1998. Before this, the MWRs were placed in tip-scan mode manually during a clear-sky period, and 1–3 days of tip-curve data were collected. These data were then used to calibrate the MWR. These manually collected calibration datasets were typically used for months at a time before being updated. As discussed previously, the new autocalibration software collects and reduces tip-curve data autonomously whenever the sky is determined to be clear; this maintains the calibration of this instrument to approximately 0.3 K. This approach may add a small amount of noise in the calibration if the instrument is truly stable over long periods of time. However, due to the infrequency of the manually collected tip-curve data, the calibration of the MWR data prior to October 1998 has a larger uncertainty than the more recent data.

A final source of uncertainty in the original QME

dataset collected before June 1995 is in the AERI observations themselves. In 1993, the prototype AERI-00 (the same instrument used during SPECTRE) was placed at the ARM facility inside a trailer, viewing the sky through a ''chimney'' that protected the instrument from the elements (Revercomb et al. 1996; Knuteson et al. 1999). This instrument, which used liquid nitrogen to cool the detectors, was replaced with the operational AERI-01 in June 1995, which was the first AERI to incorporate a Stirling cooler. However, a side-by-side comparison of the two systems performed when the AERI-01 was first installed revealed that the chimney implementation induced a small obstruction to the instrument's field of view (Knuteson et al. 1999). The coincident observations by the two AERI systems allowed a correction to be derived to account for the obstruction in the prototype system; however, the uncertainty in this corrected data is somewhat larger than the uncertainty in normal AERI observations (Revercomb et al. 1996; Shen and Ellingson 1996).

Operationally, the ARM program runs the LBLRTM twice for each QME sample: once with the original radiosonde profiles and once with a radiosonde water vapor profile that has been scaled to agree in PWV with the MWR using an altitude independent scale factor. For the 1994–97 QME dataset, the version of the LBLRTM was 5.10, the spectroscopic line database was HITRAN 1996 (Rothman et al. 1998), and the water vapor continuum model used was CKD 2.4 (Clough et al. 1989; Han et al. 1997; Tobin et al. 1999). After carefully screening the data in an attempt to remove QME cases that may be contaminated with cirrus clouds, the resulting dataset (shown in Fig. 2) contains 743 samples that cover a wide range of PWV during both the day and night. The large errors in the strengths of the water vapor lines are easily seen as spikes in the three spectral residual panels (Figs. 2a–c). There also appears to be a dependence of the radiance residual on PWV in the continuum absorption (as indicated by the plot of the residuals at 900 cm^{-1} in Fig. 2d). However, the uncertainties in the atmospheric state and radiometric observations, and in particular the calibration of the MWR, as well as the possibility that several cases could still be cloudy, prevented us from attempting to modify the water vapor continuum model based on these results (Brown et al. 1997; Ellingson and Shen 1997; Ellingson 1998; Clough et al. 1999).

The 1994–97 QME dataset is a very valuable dataset, however. Analysis of this dataset led to the water vapor IOPs, which then led to many important improvements that reduced the uncertainties in the routine water vapor observations (Ellingson 1998). These improvements included the much more frequent tip-curve calibrations and the beamwidth correction on the MWR, the aspiration of the radiosondes before launch, and the need to scale them to the MWR. It also highlighted the importance of using the depolarization capability of the Raman lidar for cirrus detection.

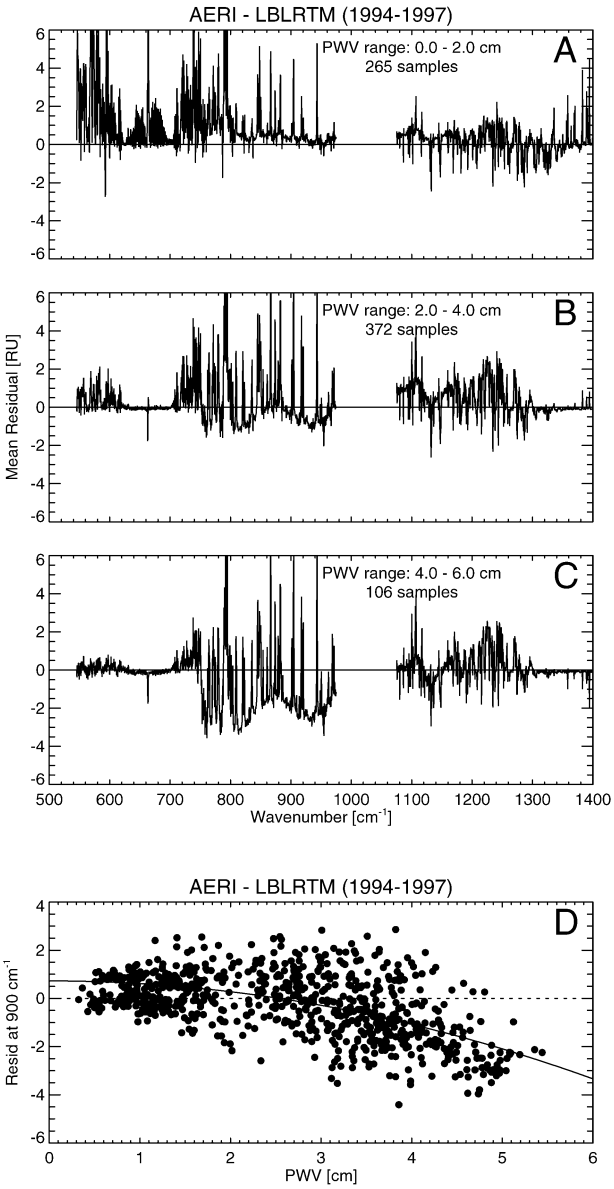

FIG. 2. Mean spectral residuals (AERI − LBLRTM) for the 1994–97 QME dataset, separated into three PWV ranges: (a) 0–2, (b) 2–4, and (c) 4–6 cm. The LBLRTM version is 5.10, the spectroscopic line database is HITRAN 1996, and the water vapor continuum module is CKD 2.4. Cirrus cases were removed by identifying them with threshold tests; however, there may be some cases that are still cloud contaminated in this dataset. Large errors in the water vapor line parameters in HITRAN 1996 are easily seen as spikes in these plots. Note that the region of strong ozone absorption between 980 and 1080 cm^{-1} is not displayed because ARM does not routinely measure ozone column amounts at the SGP site. (d) The residuals are a function of PWV, which is highlighted by the mean spectral residual at 900 cm^{-1}.

4. Creation of a new QME dataset: 1998–2001

As described in section 3, the combination of uncertainties in the AERI observations, MWR calibration, and cirrus cloud detection made it difficult to use the

TABLE 1. Distribution of samples per month for the new QME.

Month	No. of samples	Month	No. of samples
Jan	6	Feb	6
Mar	36	Apr	20
May	15	Jun	3
Jul	8	Aug	11
Sep	34	Oct	54
Nov	12	Dec	25

1994–97 QME dataset for its original intent: to evaluate the LBLRTM quantitatively. Improvements made to the various instruments and the data streams resulting from the original analysis allowed us to generate a new QME that would address most of the issues that limited the original QME dataset. The new QME dataset consists of nighttime, clear-sky cases from October 1998 to September 2001 where the AERI, MWR, radiosonde, and Raman lidar are all operating well. The Raman lidar, AERI, and MWR data are 30-min averages starting from the sonde launch time. The nighttime constraint ensured that the signal-to-noise in the Raman lidar data was at a maximum, and so the depolarization ratio could be used eliminate cases corrupted by thin cirus. Any height bin with a Raman lidar measured depolarization ratio greater than 7% was classified as a cirrus cloud. During this time period, the MWR was collecting tip-scan curves whenever the scene was determined to be clear, and we have further restricted the QME dataset to include only those times when the tip-scan curve showed that the atmosphere was horizontally (in the vertical plane) homogeneous. The sky was considered homogeneous if the standard deviation of the equivalent zenith sky brightness temperatures (Han and Westwater 2000) was less than 0.30 and 0.25 K in the 23.8- and 31.4-GHz channels, respectively. Including only samples associated with valid tip curves into the QME would also allow the nominal calibration method described in Liljegren (2000) to be compared to results where the instrument was instantaneously calibrated using each individual tip-curve dataset.

The dataset that resulted consists of 230 samples. The monthly distribution of the samples is given Table 1. During this period of time, typically only one radiosonde was launched at night (and none on the weekends), and with the stringent screening process used, many of these samples were not included. During some months (notably March/April and September/October) there are significantly more cases; this is due to special radiosonde launches during IOPs that increased the probability of finding samples that met our criteria. Furthermore, the SGP has more clear-sky episodes during autumn than other seasons, which also contributes to these statistics.

The ranges of PWV, surface temperature, and aerosol optical thickness (AOT) that are covered by this dataset are given in Fig. 3. There are questions regarding the impact of aerosols on the longwave radiative flux at the SGP site (Whitney et al. 1996) and the simultaneous observations of water vapor and aerosols by the Raman lidar will be used to address this question. The correlation between surface temperature and PWV ($r^2 = 0.68$) is expected, as warmer surface conditions are generally associated with warmer, more moist atmospheres. The PWV and AOT also show fair correlation ($r^2 = 0.45$). There are more observations at lower water vapor amounts due to the increased number of samples from the spring and late autumn period as opposed to the summer months. However, it should be noted that the data collection from these instruments is ongoing, and thus the size of the dataset continues to grow and cover an even wider range of atmospheric conditions.

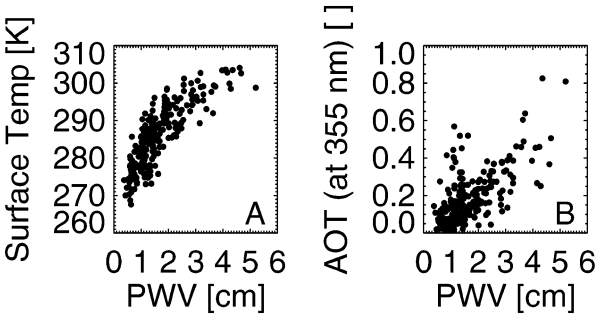

FIG. 3. Scatterplots showing (a) the distribution of surface temperature and (b) aerosol optical thickness as a function of PWV for the 1998–2001 QME dataset.

The LBLRTM calculations for the new QME dataset use the latest release of the HITRAN spectroscopic database (HITRAN 2000 update 01). Laboratory observations of water vapor absorption led to changes in this database, with the largest changes from the HITRAN 1996 database in the water vapor lines occurring in the spectral region from 10–20 μm. These changes result in a significant improvement in the ''online'' spectral residuals between the AERI observations and the LBLRTM calculations (Fig. 4). A discussion of the changes between HITRAN 1996 and 2000 can be found in Toth (1998, 2000), Rothman et al. (2003), and Newman and Taylor (2002). The version of the LBLRTM model used for these runs is 6.01, and the water vapor continuum absorption model is CKD 2.4.

5. Analysis of the new QME dataset: 1998–2001

As discussed in sections 2c and 2d, the calibration of the radiosonde moisture profile exhibits large sonde-to-sonde variability, which translates directly to large variability in the observed minus calculated radiance residuals. We use a height-independent scale factor derived by comparing PWV retrieved from coincident MWR data to the radiosonde's PWV to reduce this calibration variability. However, any uncertainties in the MWR's calibration and/or its retrieval model are introduced into the profile. Therefore, this section will investigate the impact on the QME residuals for two MWR

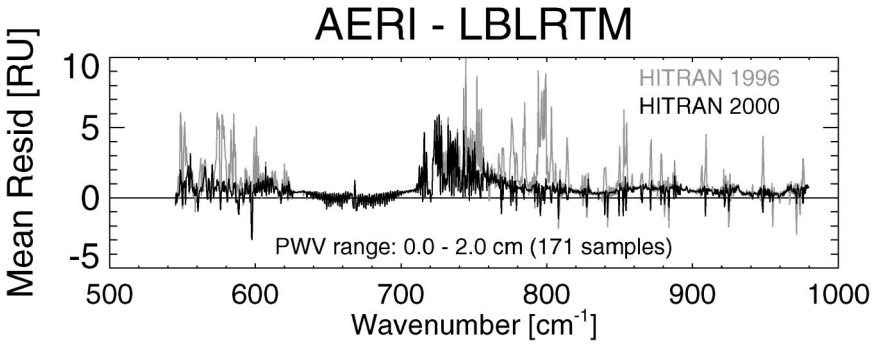

FIG. 4. Mean spectral residuals between the AERI and the LBLRTM calculations using the HITRAN 1996 (gray) and HITRAN 2000 (black) spectroscopic databases for the low water cases (0–2 cm of PWV) in the new QME dataset. The improvement in the spectral residuals due to the improvements of the water vapor absorption line parameters in the database is significant.

calibration techniques, different PWV retrieval techniques, and different microwave absorption models.

The autocalibration software derives the MWR's noise diode temperature from a linear regression of the temperature of the blackbody against the noise diode's calibrated temperature (Liljegren 2000). The regression is built from a rolling set of successful tip scans (~3000), so when a new tip scan is evaluated and deemed to be a good calibration point, it is added to the database, the oldest sample is removed, and the regression is recomputed. All of the samples in the new QME dataset were selected after the MWR autocalibration software was installed, and thus there are tip scans for each QME sample. These data have been reduced to derive the instantaneous calibration for each observation. PWV was then retrieved from these instantaneously calibrated brightness temperatures, and the results compared against the nominally calibrated results. Typical differences between the two calibration techniques for an entire clear-sky day are shown in Fig. 5. The mapping of the off-zenith brightness temperatures to zenith for the instantaneous calibration method implies a spatial average, which is why the small-scale variations are smoothed out. A statistical comparison of the PWV retrieved from the nominally calibrated versus instantaneously calibrated MWR data used in the 1998–2001 QME are given in Table 2. The nominally calibrated MWR can lead to 1%–3% differences in retrieved PWV (Table 2, Fig. 5), as compared to the instantaneously calibrated observations.

In addition to using the nominal quasi-statistical retrieval of PWV based upon the Liebe87 model as described in section 2c, a physical retrieval was also developed. The radiosonde profile was used to specify the atmospheric structure, and the mixing ratio profile was scaled in an iterative manner until the brightness temperature at 23.8 GHz calculated by the absorption model agreed with the observed brightness temperature to within 0.1%. Two contemporary absorption models were used in this process: Liebe87 and Rosenkranz98 (Rosenkranz 1998).

A final set of MWR data was also computed. Unscaled radiosonde profiles were input into the absorption models to compute the 23.8-GHz brightness temperature, and the observed minus computed brightness temperature residuals were used to determine a zero PWV bias. This bias was approximately 0.6 K for the Rosenkranz98 model. The cause of this small bias is currently under investigation and is attributed to a combination of small offset calibration errors in the MWR and uncertainties in the dry component of the microwave absorption models, such as oxygen absorption. Without removal of this bias, simultaneous retrievals of both liquid water and water vapor in clear-sky scenes often result in negative values of liquid water; with the bias removed, the liquid water retrievals are more physical. After this bias was subtracted from the observed brightness temperatures, physical retrievals were again performed with the Rosenkranz98 model.

Statistics for the various MWR-retrieved PWV are given in Table 2. All of the various sources of PWV are compared to the operational MWR data stream, which uses the automated calibration routine, the quasi-statistical retrieval and Liebe 87 as specified in section 2c. The results demonstrate that there are no significant differences between using a physical or the quasi-statistical retrieval method, or between the operationally calibrated versus instantaneously calibrated brightness temperatures. Both the unscaled radiosondes and the retrievals where the brightness temperature offset were removed before the retrieval show an approximate 4% dry bias compared to the other retrievals. Furthermore, there is significantly more variability in the comparison with the radiosondes than the other retrieval methods.

Using these various MWR products, many sets of LBLRTM calculations were made for the new QME dataset with the input moisture profiles being from the Raman lidar or radiosonde profiles that have been scaled

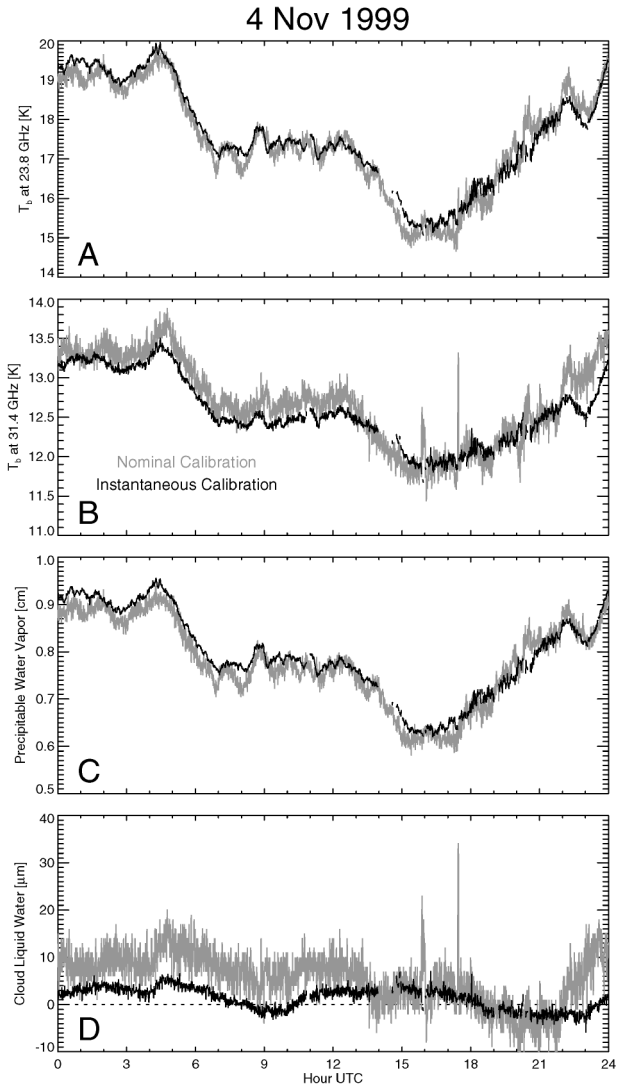

FIG. 5. (a), (b) Comparison of the 23.8- and 31.4-GHz brightness temperatures, as well as (c) the retrieved PWV and (d) cloud liquid water, for a clear-sky day at SGP (4 Nov 1999). The gray traces are where the autocalibration software (Liljegren 2000) determined the calibration for each sample. The black curves show the results where the tip-curve data at each sample was processed to yield instantaneous calibration factors.

TABLE 3. Water vapor inputs for each set of LBLRTM runs.

Case	Water vapor input into LBLRTM
A	Unscaled radiosondes
B	Radiosonde scaled with the operational MWR product (nominally calibrated, quasi-statistical Liebe87 retrieval)
C	Raman lidar scaled with the operational MWR product
D	Radiosonde scaled with the instantaneously calibrated, quasi-statistical Liebe87 retrieval
E	Radiosonde scaled with the instantaneously calibrated, physical Liebe87 retrieval
F	Radiosonde scaled with the instantaneously calibrated, physical Rosenkranz98 retrieval
H	Radiosonde scaled with the nominally calibrated, physical Liebe87 retrieval
J	Same as case F, but the T_b offset at 23.8 GHz was removed before the retrieval

to agree with the MWR products. Table 3 provides the details on the various inputs. It should be noted that cases A and B are routinely created by the ARM program and are thus in the ARM data archive.

Before comparing the various LBLRTM ensembles against the AERI observations, we compared each ensemble to case ''B'' to gauge the impacts of the different MWR retrievals. The results are summarized in Fig. 6. The first thing to note is that the unscaled radiosonde results (case ''A'') have by far the most variability as compared to the baseline case (B), with almost 3 times as much variability at 800 cm^{-1} as any of the other cases. This was expected due to the significantly higher rms for radiosondes versus the MWR retrieval in Table 2, attributable to the inherent sonde-to-sonde variability in the calibration of the moisture sensors. Compared to case B, the unscaled radiosondes (case A) and the sondes that have been scaled with the retrieval where the MWR brightness temperature offset was removed beforehand (case J) are considerably drier. In a mean sense, the cases in which the radiosonde was scaled by the quasi-statistical Liebe87 retrieved product (cases B and D) agree well with each other, which means the operational calibration routine does not introduce any bias as compared to the instantaneous calibration method. However, the two retrievals (cases B and D) are obviously not identical as indicated by the small standard deviation in

TABLE 2. Statistical comparisons of PWV retrieved from the MWR with different absorption models, calibration methods, and retrievals techniques with the operational MWR product described in section 2b (automated calibration, quasi-statistical retrieval using Liebe87) for the 230 cases in the 1998–2001 QME.

Retrieval type	Calibration method	Model	Bias removed (yes/no)	Offset (cm)	Slope	Mean bias (cm)	Mean ratio	Rms (cm)
Radiosonde				−0.024	0.986	0.048	1.038	0.117
Physical	Automated	Liebe87	No	0.029	0.987	−0.008	0.989	0.033
Quasi-statistical	Instantaneous	Liebe87	No	−0.002	1.000	0.001	1.001	0.016
Physical	Instantaneous	Liebe87	No	0.025	0.988	−0.006	0.992	0.036
Physical	Instantaneous	Rosenkranz98	No	0.004	0.997	0.001	1.000	0.035
Physical	Instantaneous	Rosenkranz98	Yes	−0.037	0.996	0.044	1.036	0.056

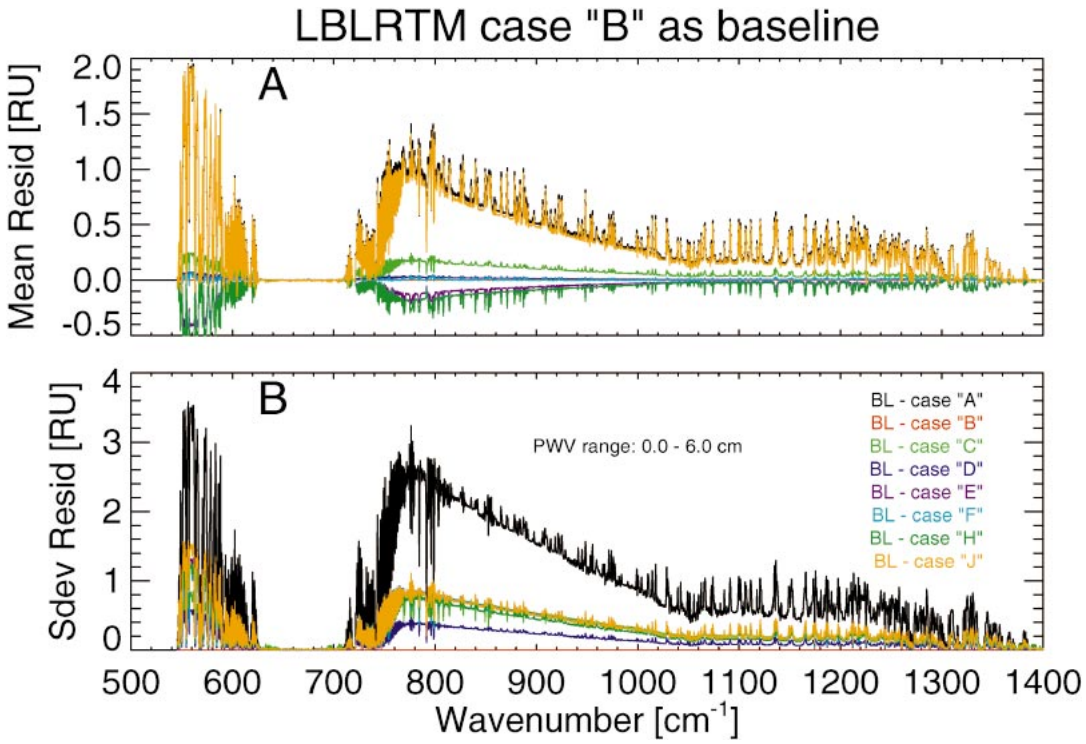

FIG. 6. (a) Mean spectral residual and (b) the standard deviation about this mean for each case in Table 3 over the 230 cases in the 1998–2001 QME, using case ''B'' as the baseline.

Fig. 6. The cases where a physical retrieval based upon Liebe87 is used to scale the radiosondes (cases E and H) show a slightly negative residual compared to the base case demonstrating that, in a mean sense, the physically retrieved values were slightly more moist. Using the Rosenkranz absorption model in the physical retrieval (case F) yields almost identical results to the baseline in terms of the mean, and the variability is almost the same as the physical retrieval that used the Liebe absorption model (case E). Interestingly, the ensemble that used the MWR-scaled Raman lidar (case C) has a slightly positive longwave residual compared to the baseline. Since the same MWR product was used to scale both the radiosonde and Raman lidar moisture profiles (cases B and C), this indicates that the Lagrangian nature of the sonde's observation does have a small impact on the calculation of radiance within the vertical column, even when averaged over a large number of cases.

Figure 6 demonstrates how the different water vapor ensembles affect the longwave radiance calculation, but does not shed light on which one is more correct in an absolute sense. In Fig. 7, these LBLRTM calculations from each ensemble are compared against the AERI observations. The mean observed minus calculated spectra for each ensemble fall into one of two groups. Cases ''A'' and ''J'' fall into the group that shows a bias of approximately 1 RU from 780 to 840 cm^{-1}, while the others fall into the group that shows little bias in this spectral region. As discussed later, this result, when looking at the means over all 230 cases, is dominated by the cases with low PWV. The 1-RU positive bias in cases A and J suggests that there is not enough absorption in the model, that the input moisture profiles are biased dry, that there is a bias in the AERI observations, or some combination of these issues. However, all of the MWR-scaled profiles, including case J where the brightness temperature offset was removed beforehand, significantly reduce the variability in the longwave residuals. Interestingly, all of the cases show an approximate 1 RU bias between 1100 and 1300 cm^{-1}, which is indicative of an error in the model or in the AERI observations in this region. The large residuals observed between 720 and 760 cm^{-1} are indicative of errors in the modeling of the carbon dioxide absorption, which has been addressed in the latest version (v7.01) of the LBLRTM (Shephard et al. 2003).

The AERI observations have uncertainties associated with them, and so questions that arise are: 1) What are the size of these uncertainties? and 2) Are these uncertainties too large to distinguish between 1-RU differences in the modeled results? To estimate the uncertainty in the AERI observation, uncertainties in the blackbody temperatures and emissivities are propagated via the linear calibration equation to derive a root sum of square error (RSS) in the observed spectrum (Knuteson et al.

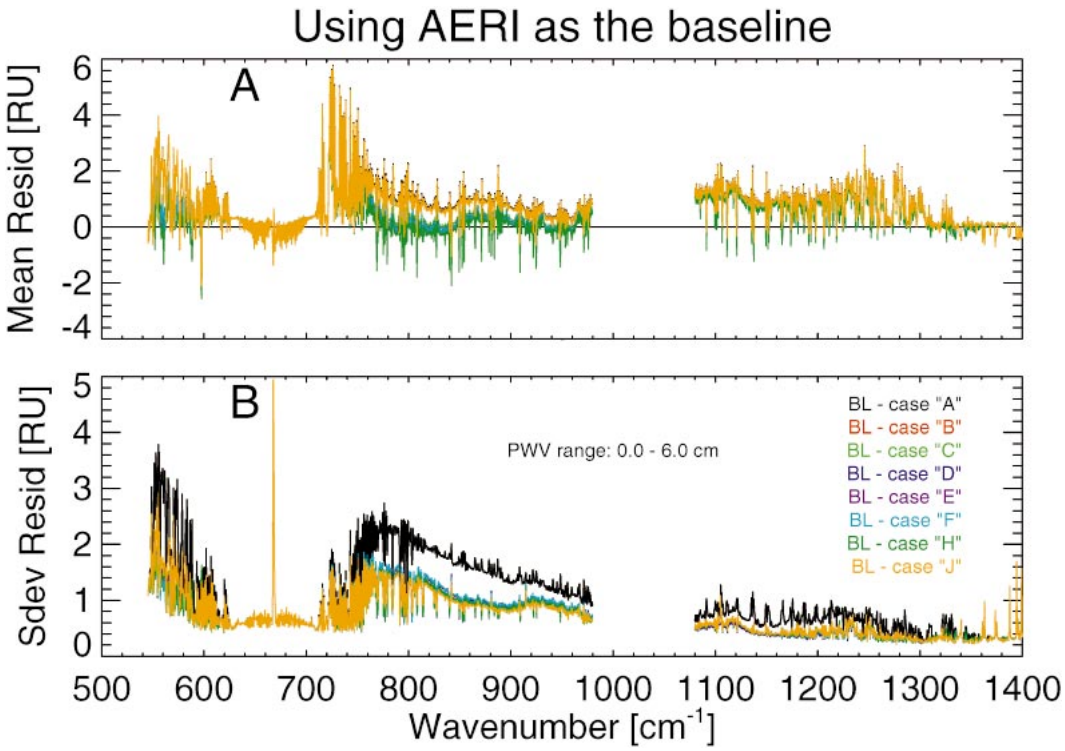

FIG. 7. (a) Mean spectral residual and (b) the standard deviation about this mean for each case in Table 3 over the 230 cases in the 1998–2001 QME, using AERI observations as the baseline.

2004b). [The uncertainty in the nonlinearity correction has been neglected here, as a 10% uncertainty in this correction translates into a 0.05-RU uncertainty at 900 cm^{-1} at 300 K (Knuteson et al. 2004b).] A typical RSS spectrum for a clear-sky AERI observation, multiplied by 100, is shown in the top panel of Fig. 8. The error in the AERI observation increases as the observed brightness temperature becomes colder than ambient, which is why the error is larger in the atmospheric window than in the center of the 15-μm (667 cm^{-1}) carbon dioxide band. The absolute magnitude of the error has a strong relationship with the temperature of the ambient blackbody (as shown in the middle panel of Fig. 8); however, typically warmer temperatures correspond to higher radiance in the atmospheric window and thus the relative error remains approximately the same. This phenomenon is demonstrated in the bottom panel of Fig. 8, where the observed minus calculated (case B) residuals at 900 cm^{-1} (actually the mean residual between 898 and 904 cm^{-1}) are shown as a function of PWV, where the error bars are the RSS errors in the AERI observations. These results demonstrate that the uncertainty in the AERI observations are on the order of 0.4 RU, and thus the 1-RU difference between the two ensemble clusters exhibited Fig. 7 is significant.

The radiance residuals at 900 cm^{-1} are investigated to quantify the variability removed by scaling the moisture profile by the various MWR products. The bottom panel of Fig. 8 shows a positive residual at low PWV amounts, little to none for intermediate water vapor amounts, and a negative residual for higher PWV amounts. Similar behavior is seen for most wavelengths between 750–1000 cm^{-1}, as shown in Fig. 9. Note this is the same basic feature seen in the 1994–97 QME dataset (Fig. 2). At these wavelengths (and away from water vapor absorption lines), the self-broadened portion of the water vapor continuum is the primary absorption mechanism, and this absorption increases as the square of the total water vapor amount. At high PWV, we conclude that the observed minus calculated radiance residuals are larger than the uncertainties associated with either the input profiles or the AERI observations. Attributing the differences solely to errors in the self-broadened water vapor continuum, we fit quadratic curves of the form (residual) $= a + b\,(\mathrm{PWV})^2$ to each ensemble. For each ensemble, we then removed the trend and computed the rms difference. These fits, along with the rms values, are given in Table 4. Considering the intercept (coefficient a), cases A and J are obviously different than the other cases as discussed previously. The physical retrievals that used the Liebe87 model have a somewhat smaller (approximately 20%) intercept than the baseline case. The curvature parameter b is similar for all cases, with no apparent dependence on forward model algorithm or retrieval technique. The rms differences for all of the cases, other than the unscaled radiosondes, are virtually the same, each being within 10% of the other cases.

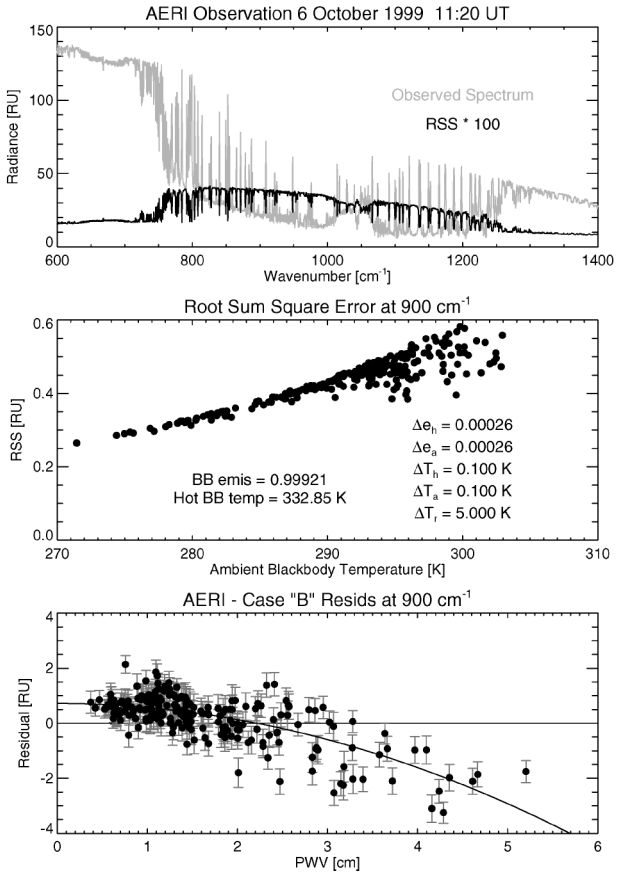

FIG. 8. (top) The RSS error (in black), multiplied by 100, for a typical clear-sky AERI observation (in gray). (middle) The relationship of the RSS error at 900 cm^{-1} with the ambient temperature for the 1998–2001 QME dataset. (bottom) The mean observed minus calculated (case B) residual at 900 cm^{-1} for the 1998–2001 QME, where the error bars indicate the uncertainty (RSS errors) in the AERI observations. The coefficients for the fitted line are given in Table 4.

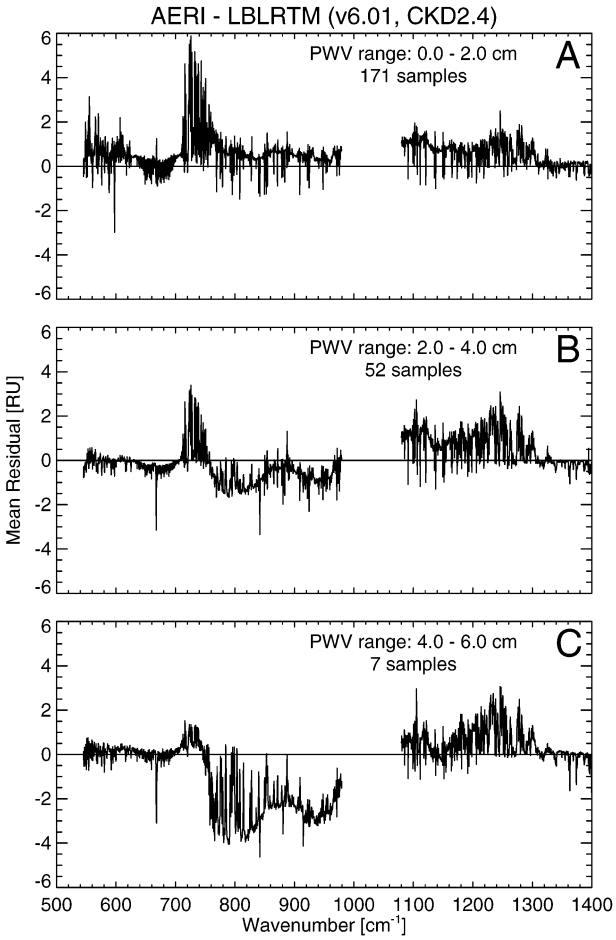

FIG. 9. Mean spectral observed minus calculated (case B) residuals for the 1998–2001 QME for three PWV ranges: (a) 0–2, (b) 2–4, and (c) 4–6 cm. Note that the LBLRTM version is 6.01, the line database is HITRAN 2000, and the water vapor continuum module is CKD 2.4.

Note that in all of the cases, there is a small offset at low PWV amounts (as indicated by the coefficient *a* in Table 4) that is slightly larger than the uncertainty in the AERI observations. One possible explanation is that there are aerosols in the atmosphere which are contributing ''extra'' signal that is not accounted for in the model. By design, this dataset was selected when the Raman lidar was operational and when the AOT at the laser wavelength (355 nm) was derived from its observations. These AOT observations show no correlation with the residuals at 900 cm^{-1} (Fig. 10). The infrared radiance residuals were also not correlated with visible aerosol optical depth measurements or with surface based in situ aerosol observations (C. Andronache 2003, personal communication). Research into the small positive radiance residual at small water vapor burdens is ongoing.

The quadratic nature of the observed minus calculated infrared residuals between 750–1000 cm^{-1} with PWV suggests that the self-broadened portion of the water vapor continuum in CKD 2.4 is too strong in this region. The fact that this behavior is observed for the different techniques used to derive PWV from the MWR suggests that the observed curvature is not due to errors in the input water vapor profiles. This is the main conclusion

TABLE 4. Coefficients for the fit of (residual) = $a + b(\text{PWV})^2$ to the residuals at 900 cm^{-1} for each of the cases in the 1998–2001 QME. The rms value, computed after the trend was removed, is also given for each case.

Case	*a*	*b*	Rms
A	1.07	−0.09	1.27
B	0.72	−0.15	0.61
C	0.73	−0.12	0.61
D	0.74	−0.15	0.62
E	0.58	−0.12	0.65
F	0.70	−0.14	0.66
H	0.54	−0.12	0.65
J	1.10	−0.11	0.62

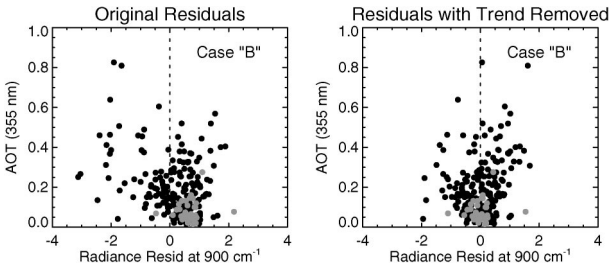

FIG. 10. Scatterplot of aerosol optical thickness measured by the Raman lidar at 355 nm (left) with the observed minus calculated (case B) residual at 900 cm^{-1}, and (right) with the trend (given by Table 4) removed for the 1998–2001 QME. Samples where the PWV is less than 0.8 cm are indicated in gray.

of this work. Additionally, the elevated residuals in the 1100–1300-cm^{-1} region indicate that the water vapor continuum absorption in CKD 2.4 is too weak in this region.

Several LBLRTM calculations were performed at high water vapor amounts (4–5 cm in PWV), where a range of scale factors was used to scale the self- and foreign-broadened components of the water vapor continuum. The mean AERI − LBLRTM residuals from the 1994–97 QME dataset were then computed for each microwindow and, following Revercomb et al. (1994), these mean residuals were used to select the best scale factor from the set of perturbed model runs (Tobin et al. 2002). However, separating the errors in continuum absorption into the self-broadened and foreign-broadened components is challenging, especially in regions of the spectrum where both contribute equally to the observed radiance (such as at 1250 cm^{-1}). Therefore, these multipliers derived from the QME dataset were used in the development of a new formulation of the water vapor continuum that has both collision induced and line shape components (Mlawer et al. 2003). This new continuum model, called MT_CKD v1.0, has these

TABLE 5. Multipliers for the self- (C_s^0) and foreign-broadened (C_f^0) water vapor continuum in CKD 2.4 derived from the MT_CKD continuum.

Wavenumber	C_s^0 multiplier	C_f^0 multiplier	Wavenumber	C_s^0 multiplier	C_f^0 multiplier
600.0	1.099	0.723	1010.0	1.024	22.042
610.0	1.083	0.732	1020.0	1.038	20.598
620.0	1.068	0.767	1030.0	1.054	18.307
630.0	1.055	0.859	1040.0	1.072	16.231
640.0	1.044	0.909	1050.0	1.083	15.654
650.0	1.030	1.000	1060.0	1.079	15.027
660.0	1.019	1.123	1070.0	1.065	13.959
670.0	1.014	1.246	1080.0	1.059	12.949
680.0	1.008	1.340	1090.0	1.052	12.819
690.0	1.008	1.461	1100.0	1.044	12.936
700.0	1.000	1.639	1110.0	1.036	12.445
710.0	0.981	1.773	1120.0	1.037	12.765
720.0	0.961	1.941	1130.0	1.038	12.545
730.0	0.944	2.307	1140.0	1.039	11.562
740.0	0.931	2.986	1150.0	1.050	10.240
750.0	0.919	3.481	1160.0	1.062	8.786
760.0	0.918	3.691	1170.0	1.074	7.472
770.0	0.916	3.726	1180.0	1.083	6.281
780.0	0.916	3.935	1190.0	1.095	5.238
790.0	0.918	4.194	1200.0	1.104	4.478
800.0	0.920	4.265	1210.0	1.119	3.860
810.0	0.922	4.512	1220.0	1.146	3.270
820.0	0.927	4.960	1230.0	1.170	2.736
830.0	0.937	5.961	1240.0	1.180	2.257
840.0	0.946	7.371	1250.0	1.198	1.943
850.0	0.959	8.545	1260.0	1.213	1.684
860.0	0.962	9.248	1270.0	1.248	1.485
870.0	0.965	9.920	1280.0	1.257	1.296
880.0	0.969	10.743	1290.0	1.229	1.116
890.0	0.967	13.014	1300.0	1.218	1.011
900.0	0.969	14.435	1310.0	1.181	0.912
910.0	0.961	16.258	1320.0	1.162	0.869
920.0	0.946	18.497	1330.0	1.110	0.844
930.0	0.946	19.550	1340.0	1.031	0.820
940.0	0.942	20.953	1350.0	0.997	0.818
950.0	0.947	21.667	1360.0	0.928	0.821
960.0	0.961	24.132	1370.0	0.887	0.825
970.0	0.977	24.582	1380.0	0.873	0.860
980.0	0.990	24.609	1390.0	0.842	0.891
990.0	1.000	23.392	1400.0	0.855	0.931
1000.0	1.017	22.207			

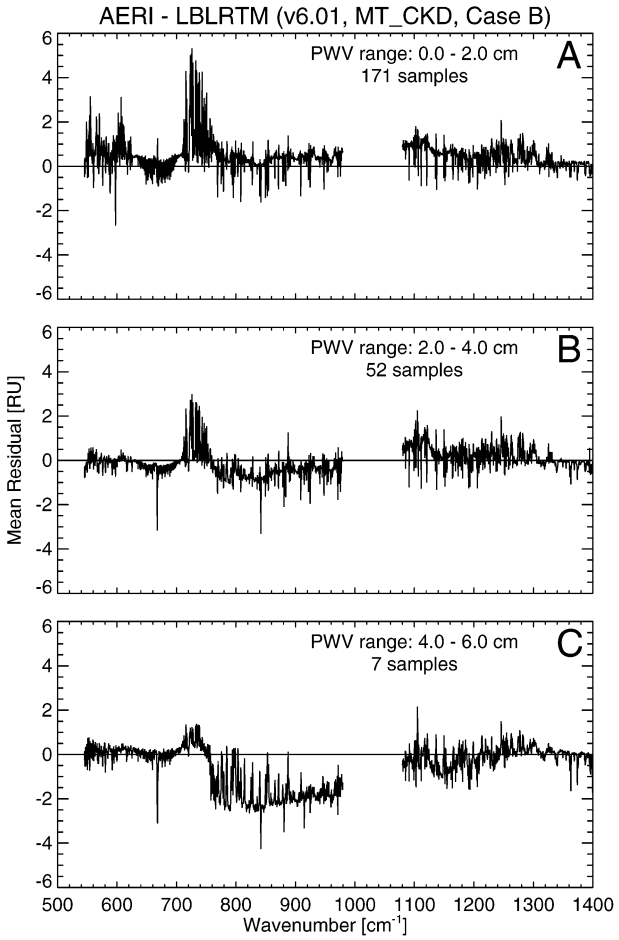

FIG. 11. Mean spectral observed minus calculated (case B) residuals for the 1998–2001 QME for three PWV ranges: (a) 0–2, (b) 2–4, and (c) 4–6 cm. Note that the LBLRTM version is 6.01, the line database is HITRAN 2000, and the water vapor continuum module is MT_CKD. Note that the broad spectral bump in the residuals between 750–1000 cm^{-1} has been eliminated with the new continuum, and that the residuals in the 1125–1325 cm^{-1} region are much smaller than the residuals shown in Fig. 9.

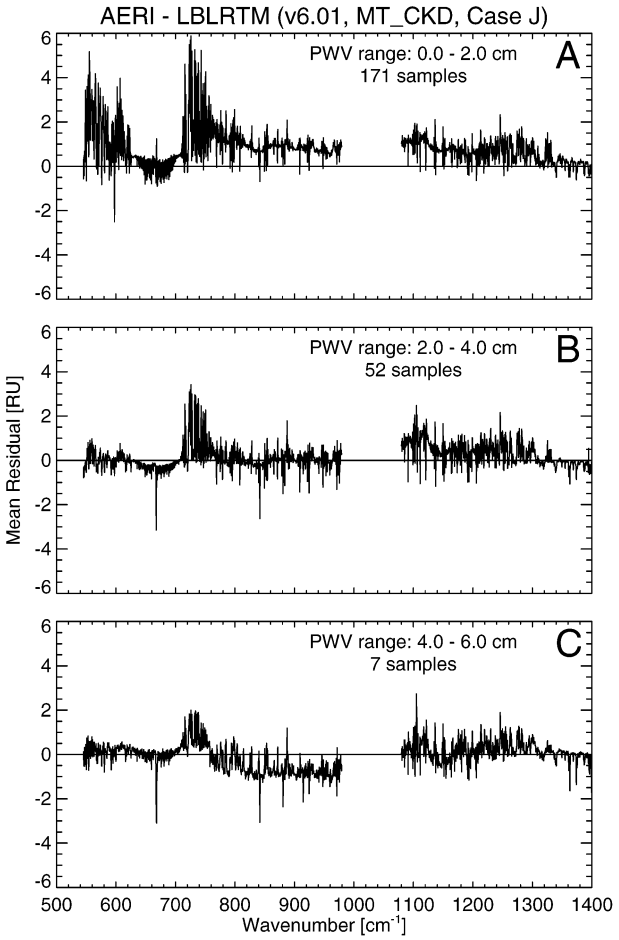

FIG. 12. Same as Fig. 11, except using case J as the input profiles.

two components applied consistently across the entire spectral domain from 0 to 20 000 cm^{-1}. It should be noted that this new continuum model was developed primarily from spectral atmospheric measurements at various wavelengths, including two cases from this QME, and that the MWR observations that were used to scale the water vapor profile had the brightness temperature offset removed first (like case J). Table 5 contains a set of multipliers that can be applied to the self- and foreign-broadened continuum absorption coefficients in CKD 2.4 to yield MT_CKD values from 600 to 1400 cm^{-1}. This analysis shows that the self-broadened continuum absorption is 3%–8% too strong in the 750–1000 cm^{-1} region and 4%–20% too weak in the 1100–1300 cm^{-1} region. The foreign-broadened continuum is also shown to be up to 25 times too weak in the center of the atmospheric window; however, the amount of absorption due to the foreign broadened continuum is so low that this is almost negligible. The changes in the foreign-broadened continuum near the edges of the atmospheric window (spectral regions less than 800 cm^{-1} and greater than 1250 cm^{-1}) are significant.

To evaluate these changes to the water vapor continuum, cases B and J from the 1998–2001 QME were rerun with the MT_CKD continuum as an independent validation. The results are shown in Figs. 11 and 12, respectively. These results, especially compared against the original results in Fig. 9, demonstrate that the ''bump'' in the residuals centered at 875 cm^{-1} has been removed, resulting in much smoother spectral residuals in the 750–1000 cm^{-1} region. The differences in the results from case B and J demonstrate the remaining uncertainty associated with the uncertainty in the water vapor amount, although we feel that case J is more representative of the true results because the treatment in the microwave is more consistent. It should be noted that recent independent studies using aircraft-based Fourier transform spectrometer observations (Taylor et al.

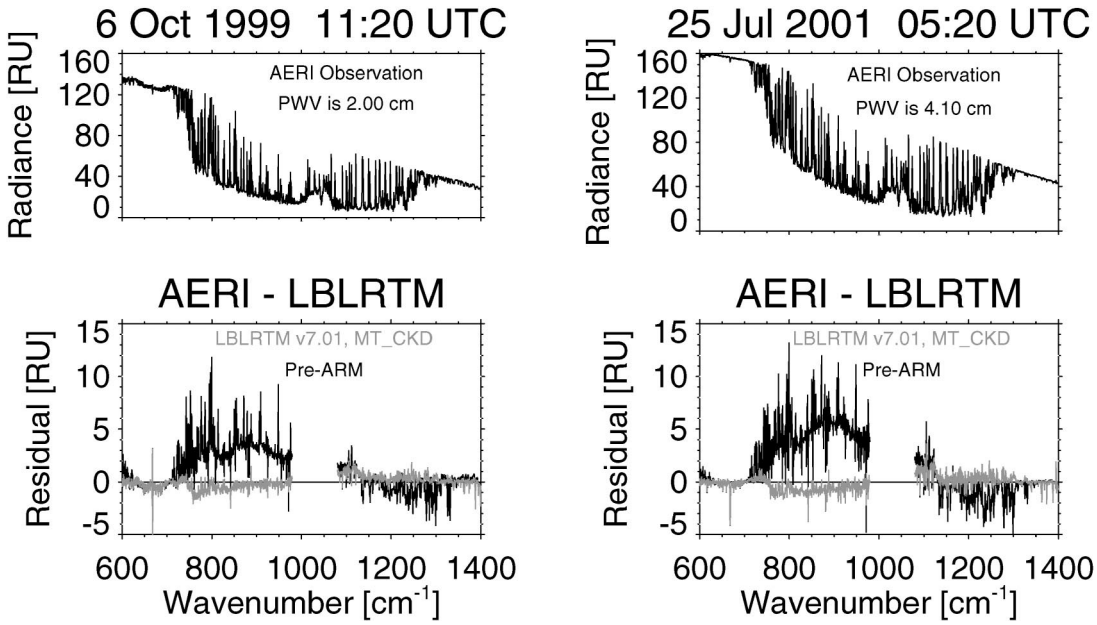

FIG. 13. (upper left) Observed AERI spectra for a midlevel (2.0 cm) and (upper right) high (4.1 cm) PWV cases, along with (lower left, lower right) observed minus calculated residuals for two different models. The residuals in black demonstrate the state of the art before ARM (i.e., in the early 1990s), utilizing the LBLRTM v5.10, HITRAN 1986, and CKD v0. In terms of downwelling longwave flux, the errors in the calculation are approximately 4.4 and 5.9 W m^{-2} for the PWV = 2.0- and 4.1-cm cases, respectively. However, some cancellation of errors occurs, and thus if we compute the error in the flux for the absolute value of the residuals, the flux errors are 5.7 and 7.6 W m^{-2}, respectively. The residuals in gray indicate the current state of the art, with the v7.01 of the LBLRTM, HITRAN 2000, and the MT_CKD water vapor continuum. The absolute value of these residuals in gray translates into 1.5 W m^{-2} errors in downwelling flux for both cases.

2003) and laboratory data (Cormier et al. 2002) reach similar conclusions regarding changes to the self-broadened continuum in the 800–1000 cm^{-1} spectral region. Our conclusions regarding the 1100–1300 cm^{-1} region, however, do not agree with those of Taylor et al. (2003). They suggest a decrease in the self-broadened continuum coefficients in this region, whereas we suggest that increases in both the foreign- and self-broadened components are required. As mentioned previously, distinguishing between self- and foreign-broadened components of the continuum absorption with atmospheric data is difficult in this spectral region, where both components contribute significantly to the total absorption coefficient. Furthermore, the CKD models do not include temperature dependence of the foreign-broadened continuum, while theoretical studies (e.g., Ma and Tipping 1992) and comparisons of continuum coefficients derived from room temperature laboratory (Tobin et al. 1996) and Arctic atmospheric (Tobin et al. 1999) data suggest that the temperature dependence is required.

6. Conclusions

The ARM program has fielded an extensive array of instrumentation at its SGP CART site to collect long-term datasets to improve the parameterization of radiation in global climate models. This program was motivated in part by the conclusions of ICRCCM, and built upon the framework provided by SPECTRE. In 1990, the LBLRTM was using the CKD v0 continuum model (Clough et al. 1989) and the HITRAN 1986 line database. ARM supported a variety of projects that led to improvements in high spectral resolution radiative transfer, including laboratory spectroscopic studies and field experiments such as the Pilot Radiation Observation Experiment (PROBE; Westwater et al. 1999) and Surface Heat Budget of the Arctic (SHEBA; Uttal et al. 2002). The laboratory studies led to improvements in the HITRAN spectroscopic database, with the largest changes in the spectral region from 7–20 μm coming in the HITRAN 2000 release. The PROBE and SHEBA experiments led to improvements in both the self-broadened (Han et al. 1997) and foreign-broadened (Tobin et al. 1999) portions of the water vapor continuum, which was further modified to incorporate a new continuum model as described in Mlawer et al. 2003. Figure 13 demonstrates the large improvement in the modeling of high spectral resolution downwelling radiation over the past decade. The two cases are chosen from the new QME for two different water vapor amounts (PWV of 2.0 and 4.0 cm). Note that the pre-ARM results had much larger errors in both the line parameters as well as the underlying continuum as compared to the current state of the art. These improvements in the longwave

modeling translate to approximately 4 and 6 W m^{-2} in downwelling longwave flux at the surface for the two cases, respectively.

This paper discusses a carefully constructed set of cases from the SGP CART site that is being used to reduce the uncertainties in the LBLRTM, and especially the water vapor continuum model. This QME dataset consists of 230 cases from 1998–2001 covering a range of atmospheric conditions at the SGP site to test and validate radiative transfer models. The primary advantage of this dataset is that many of the uncertainties that are associated with the atmospheric state have been eliminated, such as possible thin cirrus contamination and errors in water vapor. Using this dataset, we have shown that the different absorption models used to retrieve PWV from the MWR have very little impact on the longwave observed minus calculated residuals (when the retrieved PWV is used to scale the input moisture profile used in the longwave calculation). However, there is an outstanding issue related to the need to subtract a brightness temperature offset from the MWR observations before the PWV retrieval is performed, and investigation into the source of this bias is ongoing. We have also shown that tropospheric aerosols observed at the SGP CART site have no apparent correlation with the magnitude of the longwave radiance residuals, suggesting that the infrared radiance contribution from these aerosols is negligible for the conditions studied.

This dataset, together with the 1994–97 QME dataset, was used to evaluate the LBLRTM, a popular model used by the atmospheric community, and its various components. In particular, our analysis of the QME dataset demonstrated that reducing the water vapor self-broadened continuum in CKD 2.4 by 3%–8% between 750–900 cm^{-1}, increasing it by 4%–20% from 1100–1300 cm^{-1}, and modifying the foreign-broadened continuum across the spectrum resulted in significantly reduced and spectrally smoother observed minus calculated residuals. These multiplicative factors are consistent with those required to obtain the current MT_CKD continuum model from the CKD 2.4 model. It should be stressed that the analyses from this QME together with other corroborating measurements were critical in the development of the MT_CKD model. Utilizing the MT_CKD water vapor continuum model in the LBLRTM improves both the spectral shape and magnitude of the infrared radiance calculations from 600–1400 cm^{-1}.

The improvements in the water vapor continuum model and HITRAN database allow downwelling longwave fluxes to be calculated with an accuracy of better than 2 W m^{-2}. Furthermore, the spectral distribution of the LBLRTM calculated flux is correct, and there is negligible cancellation of errors. The improved spectral accuracy is important for computing the divergence of the net flux in the atmosphere (i.e., cooling rate profiles). The accuracy of the spectral radiance calculations is also critical for remote sensing applications. The observed data used in this paper are available to the general scientific community from the ARM data archive (http://www.archive.arm.gov), and we urge the use of this data in a similar manner for the validation of other radiative transfer models.

Acknowledgments. We would like to thank the many people who participated in the organization and analysis of the original QME dataset, including J. Liljegren, N. Miller, S. Shen, B. Whitney, and the many members of the ARM Instantaneous Radiative Flux working group. We would also like to thank J. Liljegren and E. Westwater for numerous conversations regarding the microwave radiometer, and B. Lesht for discussions regarding the radiosonde dataset. This research was funded by the Atmospheric Radiation Measurement (ARM) program, which is funded by the Office of Biological and Environmental Research of the U.S. Department of Energy.

APPENDIX

List of Acronyms

Acronym	Expansion
AER	Atmospheric and Environmental Research, Inc.
AERI	Atmospheric Emitted Radiance Interferometer
AOT	Aerosol optical thickness
ARM	Atmospheric Radiation Measurement
CART	Cloud and Radiation Testbed
CKD	Clough–Kneizys–Davies
DOE	Department of Energy
FASCODE	Fast Atmospheric Signature Code
GCM	Global climate model
HIS	High-Spectral-Resolution Infrared Sounder
HITRAN	High-resolution transmission
ICRCCM	Intercomparison of radiation codes in climate models
IOP	Intensive observations period
LBLRTM	Line-by-Line Radiative Transfer Model
MPL	Micropulse lidar
MT_CKD	Mlawer–Tobin Clough–Kneizys–Davies
MWR	Microwave radiometer
NIST	National Institute of Standards and Technology
PROBE	Pilot Radiation Observation Experiment
PWV	Precipitable water vapor
QME	Quality measurement experiment
Rms	Root-mean-square
RRTM	Rapid radiative transfer model
SGP	Southern Great Plains
SHEBA	Surface Heat Budget of the Arctic
SPECTRE	Spectral radiance experiment

REFERENCES

Antikaninen, V., and A. Paukkunen, 1994: Studies on improving humidity measurements in radiosondes. *WMO Tech. Conf. on Instruments and Methods of Observation*, WMO Rep. 57, 1–5.

Brown, P. D., S. A. Clough, D. D. Turner, T. R. Shippert, R. O. Knuteson, H. E. Revercomb, and W. L. Smith, 1997: The status of the quality measurement experiments in the microwave, longwave, and shortwave. *Proc. Seventh ARM Science Team Meeting*, San Antonio, TX, U.S. Dept. of Energy. [Available online at http://www.arm.gov/publications/proceedings/conf07/abstracts/brown-97.pdf.]

Campbell, J. R., D. L. Hlavka, E. J. Welton, C. J. Flynn, D. D. Turner, J. D. Spinhirne, V. S. Scott, and I. H. Hwang, 2002: Full-time, eye-safe cloud and aerosol lidar observations at Atmospheric Radiation Measurement program sites: Instruments and data processing. *J. Atmos. Oceanic Technol.*, **19,** 431–442.

Clough, S. A., and M. J. Iacono, 1995: Line-by-line calculations of atmospheric fluxes and cooling rates: Application to carbon dioxide, ozone, methane, nitrous oxide, and the halocarbons. *J. Geophys. Res.*, **100,** 16 519–16 535.

——, Y. Beers, G. P. Klein, and L. S. Rothman, 1973: Dipole moment of water vapor from Stark measurements of H_2O, HDO, and D_2O. *J. Chem. Phys.*, **59,** 2254–2259.

——, F. X. Kneizys, E. P. Shettle, and G. P. Anderson, 1985: Atmospheric radiance and transmittance. Preprints, *Sixth Conf. on Atmospheric Radiation*, Williamsburg, VA, Amer. Meteor. Soc., 141–144.

——, ——, and R. W. Davies, 1989: Line shape and the water vapor continuum. *Atmos. Res.*, **23,** 229–241.

——, M. J. Iacono, and J. L. Moncet, 1992: Line-by-line calculations of atmospheric fluxes and cooling rates: Application to water vapor. *J. Geophys. Res.*, **97,** 15 761–15 785.

——, P. D. Brown, N. E. Miller, J. C. Liljegren, and T. R. Shippert, 1994: Residual analysis of surface spectral radiances between instrument observations and line-by-line calculations. *Proc. Fourth ARM Science Team Meeting*, Charleston, SC, U.S. Dept. of Energy. [Available online at http://www.arm.gov/publications/proceedings/conf04/abstracts/24_94.pdf.]

——, ——, J. C. Liljegren, T. R. Shippert, D. D. Turner, R. O. Knuteson, H. E. Revercomb, and W. L. Smith, 1996: Implications for atmospheric state specification from the AERI/LBLRTM quality measurement experiment and the MWR/LBLRTM quality measurement experiment. *Proc. Sixth ARM Science Team Meeting*, San Antonio, TX, U.S. Dept. of Energy. [Available online at http://www.arm.gov/publications/proceedings/conf06/abstracts/cloug_96.pdf.]

——, ——, D. D. Turner, T. R. Shippert, J. C. Liljegren, D. C. Tobin, H. E. Revercomb, and R. O. Knuteson, 1999: Effect on the calculated spectral surface radiances due to MWR scaling of sonde water vapor profiles. *Proc. Ninth ARM Science Team Meeting*, San Antonio, TX, U.S. Dept. of Energy. [Available online at http://www.arm.gov/publications/proceedings/conf09/abstracts/clough-99.pdf.]

Cormier, J. G., R. Ciulyo, and J. R. Drummond, 2002: Cavity ringdown spectroscopy measurements of the infrared water vapor continuum. *J. Chem. Phys.*, **116,** 1030–1034.

Ellingson, R. G., 1998: The state of the ARM-IRF accomplishments through 1997. *Proc. Eighth ARM Science Team Meeting*, Tucson, AZ, U.S. Dept. of Energy. [Available online at http://www.arm.gov/publications/proceedings/conf08/abstracts/ellingson-98.pdf.]

——, and Y. Fouquart, 1991: The intercomparison of radiation codes in climate models (ICRCCM): An overview. *J. Geophys. Res.*, **96,** 8925–8927.

——, and W. J. Wiscombe, 1996: The spectral radiance experiment (SPECTRE): Project description and sample results. *Bull. Amer. Meteor. Soc.*, **77,** 1967–1985.

——, and S. Shen, 1997: Comparisons of surface longwave radiance between line-by-line radiative transfer model and Atmospheric Emitted Radiance Interferometer observations from the Atmospheric Radiance Measurement program. *Proc. Seventh ARM Science Team Meeting*, San Antonio, TX, U.S. Dept. of Energy. [Available online at http://www.arm.gov/publications/proceedings/conf07/abstracts/ell-97.pdf.]

——, J. Ellis, and S. Fels, 1991: The intercomparison of radiation codes in climate models (ICRCCM): Longwave results. *J. Geophys. Res.*, **96,** 8928–8953.

Goldsmith, J. E. M., F. H. Blair, S. E. Bisson, and D. D. Turner, 1998: Turn-key Raman lidar for profiling atmospheric water vapor, clouds, and aerosols. *Appl. Opt.*, **37,** 4979–4990.

Guichard, F., D. Parsons, and E. Miller, 2000: Thermodynamic and radiative impact of the correction of sounding humidity bias in the Tropics. *J. Climate*, **13,** 3615–3624.

Han, Y., and E. R. Westwater, 2000: Analysis and improvement of tipping calibration for ground-based microwave radiometers. *IEEE Trans. Geosci. Remote Sens.*, **38,** 1260–1276.

——, J. B. Snider, E. R. Westwater, S. H. Melfi, and R. A. Ferrare, 1994: Observations of water vapor by ground-based microwave radiometers and Raman lidar. *J. Geophys. Res.*, **99,** 18 695–18 702.

——, J. A. Shaw, J. H. Churnside, P. D. Brown, and S. A. Clough, 1997: Infrared spectral measurements in the tropical Pacific atmosphere. *J. Geophys. Res.*, **102,** 4353–4356.

Iacono, M. J., E. J. Mlawer, S. A. Clough, and J.-J. Morcrette, 2000: Impact of an improved longwave radiation model, RRTM, on the energy budget and thermodynamic properties of the NCAR community climate model CCM3. *J. Geophys. Res.*, **105,** 14 873–14 890.

Knuteson, R. O., B. Whitney, H. E. Revercomb, and F. A. Best, 1999: The history of the Atmospheric Emitted Radiance Interferometer (AERI) prototype during the period April 1994 through July 1995. U.S. Dept. of Energy Tech. Memo. ARM TR-001.1. [Available online at http://www.arm.gov/publications/tech_reports/tr-001.1.pdf.]

——, and Coauthors, 2004a: Atmospheric Emitted Radiance Interferometer (AERI). Part I: Instrument design. *J. Atmos. Oceanic Technol.*, in press.

——, and Coauthors, 2004b: Atmospheric Emitted Radiance Interferometer (AERI). Part II: Instrument performance. *J. Atmos. Oceanic Technol.*, in press.

Lesht, B. M., 1999: Reanalysis of radiosonde data from the 1996 and 1997 water vapor intensive observation periods: Application of the Vaisala RS-80H contamination correction algorithm to dual-sonde soundings. *Proc. Ninth ARM Science Team Meeting*, San Antonio, TX, U.S. Dept. of Energy. [Available online at http://www.arm.gov/publications/proceedings/conf09/abstracts/leshts-99.pdf.]

Liebe, H. J., and D. H. Layton, 1987: Millimeter-wave properties of the atmosphere: Laboratory studies and propagation modeling. NTIA Rep. 87-24, 74 pp.

Liljegren, J. C., 2000: Automatic self-calibration of the ARM microwave radiometers. *Microwave Radiometry and Remote Sensing of the Environment*, P. Pampaloni, Ed., VSP Press, 9 pp. [Available online at http://www.arm.gov/instruments/publications/mwr_calibration.pdf.]

——, and B. M. Lesht, 1996: Measurements of integrated water vapor and cloud liquid water from microwave radiometers at the DOE ARM cloud and raidation testbed in the U.S. southern Great Plains. *Proc. Int. Geoscience and Remote Sensing Symp. (IGARSS)*, Lincoln, NB, IEEE, 1675–1677.

Luther, F., Ed., 1984: The intercomparison of radiation codes in climate models. World Climate Program Rep. WCP-93, World Meteorological Organization, Geneva, Switzerland, 37 pp. [Available from World Meteorological Organization, 41 avenue Giuseppe Motta, Case postale N° 2300, CH-1211 Geneva 2, Switzerland.]

——, R. G. Ellingson, Y. Fouquart, S. Fels, N. Scott, and W. Wiscombe, 1988: Intercomparison of radiation codes in climate models (ICRCCM): Longwave clear-sky results. *Bull. Amer. Meteor. Soc.*, **69,** 40–48.

Ma, Q., and R. H. Tipping, 1992: A far wing line shape theory and its application to the foreign-broadened water vapor continuum absorption. III. *J. Chem. Phys.,* **97,** 818–828.

Miloshevich, L. M., H. Vomel, S. J. Oltmans, and A. Paukkunen, 2003: In-situ validation of a correction for time-lag and bias errors in the Vaisala RS80-H radiosonde humidity measurements. *Proc. 13th ARM Science Team Meeting,* Broomfield, CO, U.S. Dept. of Energy. [Available online at http://www.arm.gov/publications/proceedings/conf13/extended_abs/miloshevich-lm.pdf.]

Minnett, P. J., R. O. Knuteson, F. A. Best, B. J. Osborne, J. A. Hanafin, and O. B. Brown, 2001: The marine–atmospheric emitted radiance interferometer: A high-accuracy, seagoing infrared spectrometer. *J. Atmos. Oceanic Technol.,* **18,** 994–1013.

Mlawer, E. J., S. J. Taubnam, P. D. Brown, M. J. Iacono, and S. A. Clough, 1997: RRTM, a validated correlated-*k* model for the longwave. *J. Geophys. Res.,* **102,** 16 663–16 682.

——, S. A. Clough, and D. C. Tobin, 2003: A new water vapor continuum model: MT_CKD_1.0. *Proc. 13th ARM Science Team Meeting,* Broomfield, CO, U.S. Dept. of Energy. [Available online at http://www.arm.gov/publications/proceedings/conf13/postes_abs/P00225.stm.]

Morcrette, J.-J., S. A. Clough, E. J. Mlawer, and M. J. Iacono, 1998: Impact of a validated radiative transfer scheme, RRTM, on the ECMWF climate model and 10-day forecasts. ECMWF Research Department Tech. Memo 252, 47 pp.

Newman, S. M., and J. P. Taylor, 2002: Impact of updates to the HITRAN spectroscopic database on the modeling of clear-sky infrared radiances. *Geophys. Res. Lett.,* **29,** 1801–1804.

Revercomb, H. E., H. Buijs, H. B. Howell, D. D. LaPorte, W. L. Smith, and L. A. Sromovsky, 1988: Radiometric calibration of the IR Fourier transform spectrometers: Solution to a problem with the High-Resolution Interferometer Sounder. *Appl. Opt.,* **27,** 3210–3218.

——, F. A. Best, R. G. Dedecker, T. P. Dirkx, R. A. Herbsleb, R. O. Knuteson, J. F. Short, and W. L. Smith, 1993: Atmospheric Emitted Radiance Interferometer (AERI) for ARM. Preprints, *Fourth Symp. on Global Climate Change Studies,* Anaheim, CA, Amer. Meteor. Soc., 46–49.

——, R. O. Knuteson, W. L. Smith, F. A. Best, R. G. Dedecker, and H. B. Howell, 1994: Atmospheric Emitted Radiance Interferometer: Status and water vapor continuum results. *Proc. Fourth ARM Science Team Meeting,* Charleston, SC, U.S. Dept. of Energy. [Available online at http://www.arm.gov/publications/proceedings/conf04/abstracts/56_94.pdf.]

——, and Coauthors, 1996: Atmospheric Emitted Radiance Interferometer. Part I: Status, basic radiometric accuracy, and unexpected errors and solutions. *Proc. Sixth ARM Science Team Meeting,* San Antonio, TX, U.S. Dept. of Energy. [Available online at http://www.arm.gov/publications/proceedings/conf06/abstracts/rev_96.pdf.]

——, W. F. Feltz, R. O. Knuteson, D. C. Tobin, P. van Delst, and B. A. Whitney, 1998: Accomplishments of the water vapor IOPs: An overview. *Proc. Eighth ARM Science Team Meeting,* Tucson, AZ, U.S. Dept. of Energy. [Available online at http://www.arm.gov/publications/proceedings/conf08/abstracts/revercomb-98.pdf.]

——, and Coauthors, 2003: The Atmospheric Radiation Measurement (ARM) programs water vapor intensive observation periods: Overview, initial accomplishments, and future challenges. *Bull. Amer. Meteor. Soc.,* **84,** 217–236.

Rosenkranz, P. W., 1998: Water vapor microwave continuum absorption: a comparison of measurements and models. *Radio. Sci.,* **33,** 919–928.

Rothman, L. S., and Coauthors, 1998: The HITRAN molecular spectroscopic database and HAWKS (HITRAN Atmospheric Workstation): 1996 edition. *J. Quant. Spectrosc. Radiat. Transfer,* **60,** 665–710.

——, and Coauthors, 2003: The HITRAN Molecular Spectroscopic Database: Edition of 2000 including updates through 2001. *J. Quant. Spectrosc. Radiat. Transfer,* **82,** 5–44.

Shen, S., and R. G. Ellingson, 1996: Comparison of recalibrated Atmospheric Emitted Radiance Interferometer observations with line-by-line radiative transfer model calculations. *Proc. Sixth ARM Science Team Meeting,* San Antonio, TX, U.S. Dept. of Energy. [Available online at http://www.arm.gov/publications/proceedings/conf06/abstracts/shen_96.pdf.]

Shephard, M. W., S. A. Clough, J. Delamere, D. C. Tobin, D. D. Turner, H. E. Revercomb, R. O. Knuteson, and R. Beer, 2003: Validation of CO_2 line parameters used in temperature retrievals. *Fourier Transform Spectroscopy,* OSA Technical Digest, Optical Society of America, 128–132.

Smith, W. L., R. O. Knuteson, H. E. Revercomb, F. Best, R. Dedecker, and H. B. Howell, 1993: GB-HIS: A measurement system for continuous profiling of the boundary layer thermodynamic structure. Preprints, *Eighth Symp. of Meteorological Observations and Instrumentation,* Anaheim, CA, Amer. Meteor. Soc., J180–J183.

Spinhirne, J. D., 1993: Micro pulse lidar. *IEEE Trans. Geosci. Remote Sens.,* **31,** 48–55.

Stokes, G. M., and S. E. Schwartz, 1994: The Atmospheric Radiation Measurement (ARM) program: Programmatic background and design of the cloud and radiation testbed. *Bull. Amer. Meteor. Soc.,* **75,** 1201–1221.

Taylor, J. P., S. M. Newman, T. J. Hewison, and A. McGrath, 2003: Water vapour line and continuum absorption in the thermal infrared–Reconciling models and observations. *Quart. J. Roy. Meteor. Soc.,* **129,** 2949–2969.

Tobin, D. C., L. L. Strow, W. J. Lafferty, and W. B. Olson, 1996: Experimental investigation of the self- and N_2-broadened continuum within the v_2 band of water vapor. *Appl. Opt.,* **35,** 4724–4734.

——, and Coauthors, 1999: Downwelling spectral radiance observations at the SHEBA ice station: Water vapor continuum measurements from 17 to 26 μm. *J. Geophys. Res.,* **104,** 2081–2092.

——, D. D. Turner, H. E. Revercomb, R. O. Knuteson, S. A. Clough, and K. Cady-Pereira, 2002: Analysis of the AERI/LBLRTM QME. *Proc. 12th ARM Science Team Meeting,* St. Petersburg, FL, U.S. Dept. of Energy. [Available online at http://www.arm.gov/publications/proceedings/conf12/extended_abs/tobin-dc.pdf.]

Toth, R. A., 1998: Water vapor measurements between 590 and 2582 cm^{-1}: Line positions and strengths. *J. Mol. Spectrosc.,* **190,** 379–396.

——, 2000: Air- and N_2-broadening parameters of water vapor 604–2271 cm^{-1}. *J. Mol. Spectrosc.,* **201,** 218–243.

Turner, D. D., and J. E. M. Goldsmith, 1999: Twenty-four-hour Raman lidar water vapor measurements during the Atmospheric Radiation Measurement program's 1996 and 1997 water vapor intensive operating periods. *J. Atmos. Oceanic Technol.,* **16,** 1062–1076.

——, T. R. Shippert, P. D. Brown, S. A. Clough, R. O. Knuteson, H. E. Revercomb, and W. L. Smith, 1998: Long-term analysis of observed and line-by-line calculations of longwave surface spectral radiance and the effect of scaling the water vapor profile. *Proc. Eighth ARM Science Team Meeting,* Tucson, AZ, U.S. Dept. of Energy. [Available online at http://www.arm.gov/publications/proceedings/conf08/abstracts/turner-98.pdf.]

——, R. A. Ferrare, L. A. Heilman Brasseur, W. F. Feltz, and T. P. Tooman, 2002: Automated retrievals of water vapor and aerosol profiles from an operational Raman lidar. *J. Atmos. Oceanic Technol.,* **19,** 37–50.

——, B. M. Lesht, S. A. Clough, J. C. Liljegren, H. E. Revercomb, and D. C. Tobin, 2003: Dry bias and variability in Vaisala RS80-H radiosondes: The ARM experience. *J. Atmos. Oceanic Technol.,* **20,** 117–132.

Uttal, T., and Coauthors, 2002: Surface heat budget of the Arctic Ocean. *Bull. Amer. Meteor. Soc.,* **83,** 255–276.

Wang, J., H. Cole, D. J. Carlson, E. R. Miller, K. Beierle, A. Paukkunen, and T. K. Laine, 2002: Corrections of humidity measurement errors from the Vaisala RS80 radiosonde—Application

to TOGA COARE data. *J. Atmos. Oceanic Technol.,* **19,** 981–1002.

Warner, J. X., and R. G. Ellingson, 2000: A new narrowband radiation model for water vapor absorption. *J. Atmos. Sci.,* **57,** 1481–1496.

Westwater, E. R., and Coauthors, 1999: Ground-based remote sensor observations during PROBE in the tropical western Pacific. *Bull. Amer. Meteor. Soc.,* **80,** 257–270.

Whitney, B. A., H. E. Revercomb, R. O. Knuteson, F. A. Best, and W. L. Smith, 1996: Atmospheric Emitted Radiance Interferometer. Part II: Water vapor and atmospheric aerosols. *Proc. Sixth ARM Science Team Meeting,* San Antonio, TX, U.S. Dept. of Energy. [Available online at http://www.arm.gov/publications/proceedings/conf06/abstracts/whitn_96.pdf.]